

Transient high-Rayleigh-number thermal convection with large viscosity variations

By ANNE DAVAILLE AND CLAUDE JAUPART

Laboratoire de Dynamique des Systèmes Géologiques, Université de Paris 7 et Institut de Physique du Globe, 4 place Jussieu, 75252 Paris Cedex 05, France

(Received 27 April 1992 and in revised form 30 November 1992)

The characteristics of thermal convection in a fluid whose viscosity varies strongly with temperature are studied in the laboratory. At the start of an experiment, the upper boundary of an isothermal layer of Golden Syrup is cooled rapidly and maintained at a fixed temperature. The fluid layer is insulated at the bottom and cools continuously. Rayleigh numbers calculated with the viscosity of the well-mixed interior are between 10^6 and 10^8 and viscosity contrasts are up to 10^6 . Thermal convection develops only in the lower part of the thermal boundary layer, and the upper part remains stagnant. Vertical profiles of temperature are measured with precision, allowing deduction of the thickness of the stagnant lid and the convective heat flux. At the onset of convection, the viscosity contrast across the unstable boundary layer has a value of about 3. In fully developed convection, this viscosity contrast is higher, with a typical value of 10. The heat flux through the top of the layer depends solely on local conditions in the unstable boundary layer and may be written

$$Q_s = -Ck_m(\alpha g/\kappa\nu_m)^{\frac{1}{3}}\Delta T_v^{\frac{4}{3}},$$

where k_m and ν_m are thermal conductivity and kinematic viscosity at the temperature of the well-mixed interior, κ thermal diffusivity, α the coefficient of thermal expansion, g the acceleration due to gravity. ΔT_v is the ‘viscous’ temperature scale defined by

$$\Delta T_v = -\frac{\mu(T_m)}{(d\mu/dT)(T_m)},$$

where $\mu(T)$ is the fluid viscosity and T_m the temperature of the well-mixed interior. Constant C takes a value of 0.47 ± 0.03 . Using these relations, the magnitude of temperature fluctuations and the thickness of the stagnant lid are calculated to be in excellent agreement with the experimental data. One condition for the existence of a stagnant lid is that the applied temperature difference exceeds a threshold value equal to $(2\Delta T_v)$.

1. Introduction

In many industrial and natural systems, thermal convection occurs in fluids whose viscosity varies strongly with temperature. For example, in geological reservoirs such as the Earth’s mantle and magma chambers, temperature differences are typically of several hundreds of degrees, implying viscosity variations of many orders of magnitude. Such convecting systems have been studied in the Rayleigh–Bénard configuration for a restricted range of viscosity contrasts, i.e. ratios, and Rayleigh numbers.

Marginal stability analyses have shown that flow develops preferentially in the least viscous parts of the fluid layer (Schubert, Turcotte & Oxburgh 1969; Stengel, Oliver & Booker 1982; White 1988). For finite-amplitude convection, theoretical efforts have been restricted to simple models in which an isothermal core flow is matched to boundary-layer flows using various assumptions. With this method, Morris & Canright (1984) and Fowler (1985) derived a scaling relationship for the heat flux, but did not specify its domain of validity. Recent numerical experiments have documented the three-dimensional planform of convection (Busse & Frick 1985; Christensen & Harder 1991). Ogawa, Schubert & Zebib (1991) identified two different regimes of convection depending on the behaviour of the upper boundary layer, which may be either involved in convective motions or stagnant in parts. These regimes were called the 'whole-layer' and 'stagnant lid' modes of convection, in agreement with earlier suggestions (Stengel *et al.* 1982; Jaupart & Parsons 1985). In these numerical studies, a few values of the Nusselt number are reported.

In laboratory experiments, the largest viscosity contrast studied was 10^5 , at a Rayleigh number of 10^4 (Booker 1976; White 1988; Stengel *et al.* 1982; Oliver & Booker 1983; Richter, Nataf & Daly 1983). Heat flux measurements have been interpreted in terms of a power-law relationship with the Rayleigh number (Booker & Stengel 1978; Richter *et al.* 1983). This relationship has been calibrated for Rayleigh numbers up to ten times critical, outside the range of values for many cases of practical interest.

Available results cannot be extrapolated with confidence because of the limited parameter range investigated. For example, in magma reservoirs which are of interest to us, Rayleigh numbers typically exceed 10^9 (Huppert & Sparks 1988; Huppert & Turner 1991). Further, these reservoirs evolve in transient regimes as they lose heat to the surrounding colder rocks. The present study aims at providing an extensive set of experimental measurements on transient convection at high viscosity contrast and high Rayleigh numbers, and to establish scaling laws for the most important variables: surface heat flux, thickness of the stagnant lid, effective temperature difference which drives convection. The basic situation investigated is that of an initially isothermal fluid layer which is impulsively cooled from above. These particular cooling conditions allow us to reach large viscosity contrasts across the unstable boundary layer. For a given temperature difference, steady-state Rayleigh–Bénard convection results in two boundary layers at the top and the bottom of the fluid layer, with each one having only part of the total temperature difference. We have been able to reach a viscosity contrast of 10^6 , which may be compared to the maximum value of 10^4 across the upper boundary layer in the Rayleigh–Bénard calculations of Ogawa *et al.* (1991).

The plan of the paper is the following. In §2, the apparatus and experimental techniques are described. Quantitative methods used to extract information from temperature measurements are explained in §3. Section 4 is devoted to a general description of the evolution of convection in the fluid layer. In §5, the heat flux data are analysed with a local dimensional analysis in the thermal boundary layer. Scaling laws for the variables of interest are derived and verified against the experimental data.

2. Experimental set-up

2.1. Apparatus and working fluids

We built a Plexiglas tank with internal dimensions of $30 \times 30 \times 20$ cm and 3 cm thick walls (figure 1). The relevant aspect ratio is that of the width of the tank over the thickness of the unstable boundary layer, which has a typical value of 30. The tank was

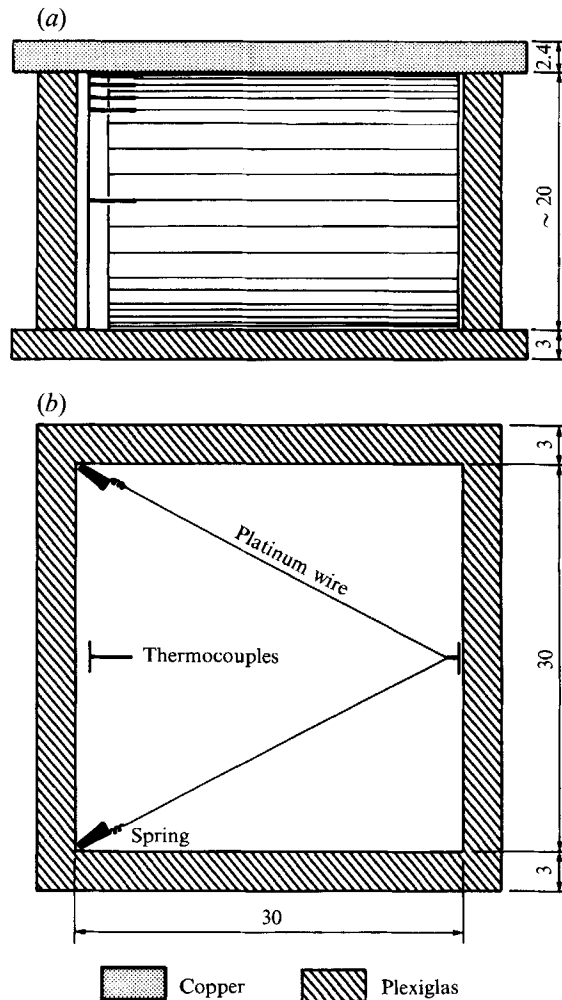


FIGURE 1. The experimental system, with all dimensions in cm: (a) side view, (b) top view. Temperature measurements are made with 19 platinum wires stretched across the tank and 5 thermocouples, with coordinates given in table 3. The tank is surrounded by Styrofoam walls and is placed in a Styrofoam enclosure, which isolates it from the laboratory.

covered with Styrofoam plates 4 cm thick and the whole set-up was placed in a Styrofoam enclosure with walls 4 cm thick, which isolates it from the laboratory. At the upper boundary of the tank, a copper plate 2.4 cm thick with an inner circulation system was connected to a powerful cooler. The lower boundary was made of Plexiglas plate 3 cm thick underlain by a layer of Styrofoam 8 cm thick, which approximates a bottom boundary condition of zero heat flux.

We used three working fluids. One was pure Golden Syrup, manufactured by Tate & Lyle Co. In order to achieve higher Rayleigh numbers, we also used Golden Syrup diluted with 10 wt. % water. The third fluid was silicone oil whose viscosity depends weakly on temperature. Unfortunately, in experiments with the latter two fluids, resolution of the boundary-layer structure was less satisfactory, and heat flux estimates were affected by larger error levels. These experiments were mostly used to study the onset of convection. All the relevant physical properties were measured in our laboratory (Appendix A; table 1; figure 2). The viscosity function for Golden Syrup

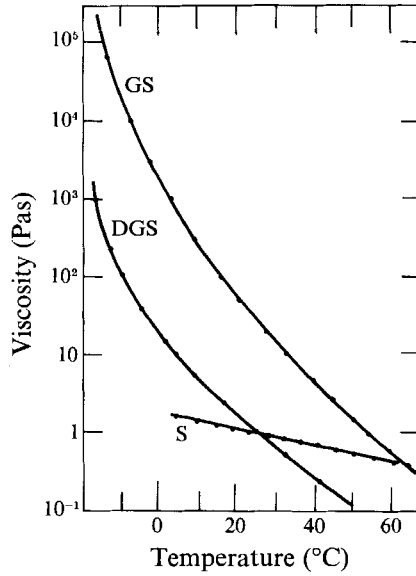


FIGURE 2. Viscosity as a function of temperature for Golden Syrup (GS), Golden Syrup diluted with 10 wt. % water (DGS), and 47V1000 Silicone oil (S).

	Silicone oil 47V1000	Golden Syrup (GS)	Diluted Golden Syrup (GSD)
Coefficient of thermal expansion α (K^{-1}) $\pm 1\%$	3.45×10^{-4}	4.33×10^{-4}	4.59×10^{-4}
Density at 20 °C ρ_0 (kg m^{-3}) $\pm 1\%$	9.7×10^2	1.438×10^3	1.384×10^3
Thermal diffusivity κ ($\text{m}^2 \text{s}^{-1}$) $\pm 5\%$	1.05×10^{-7}	1.21×10^{-7}	1.10×10^{-7}

TABLE 1. Physical properties of the working fluids

is not exponential (figure 2), which will prove useful. We have carefully measured the thermal conductivity of Golden Syrup because Richter *et al.* (1983) have questioned the accuracy of values used by Wray (1978) and White (1988). Our measurements are slightly different at low temperatures (Appendix A). For consistency with White (1988), results are given first with Wray's conductivity values. However, we consider that our conductivity determinations are more accurate and use them in the final presentation of the results.

2.2. Experimental conditions

Starting from a layer of fluid at a uniform temperature T_1 , the copper plate at the upper boundary was connected to a cooling bath at time $t = 0$. The upper boundary temperature was lowered to a fixed value $T_b = T_1 - \Delta T$ in a short time (from 2 to 6 minutes depending on the magnitude of the temperature drop). Convective motions were generated at the upper boundary, through repeated instabilities of the thermal boundary layer. The lower boundary was kept thermally insulated and hence the fluid layer was continuously cooled during an experiment. When the viscosity contrast was large, the uppermost part of the boundary layer remained stable and behaved as a stagnant lid overlying the actively convecting layer.

The initial conditions were such that the tank, its walls and the enclosure were at the same temperature T_i . The room temperature was colder, typically at 22 °C. In an experiment, the cooling fluid layer exchanges heat with the tank walls. In time $\tau = d^2/\pi\kappa$, which is 2.7 h for the Plexiglas/Styrofoam wall assemblage, the cooling effect propagates to the outer wall surface. This outer surface is in the air gap within the encasing Styrofoam box, where the temperature remains close to the initial value. For the duration of an experiment, which is typically 3 h, heat losses to the room are therefore negligible and the fluid layer only gains heat from the walls. This is a very small fraction of the heat budget for the layer because of the reduced temperature difference and the low heat capacity of the walls. This was verified with heat flux measurements (see §3.1).

The dimensionless numbers which characterize the experiments can be derived from the Oberbeck–Boussinesq equations and the viscosity function. Relevant physical properties are density at the reference temperature (ρ_0), the coefficient of thermal expansion (α), thermal capacity (C_p) and viscosity (μ). We introduce the following scales:

temperature	$\Delta T_i = T_i - T_b$ (the initial temperature difference),
viscosity	$\mu_i = \mu(T_i)$,
length	d ,
time	d^2/κ ,
pressure	$\mu_i \kappa/d^2$.

The dimensionless form of the momentum equation, which will be of interest in the discussion, is

$$\frac{1}{Pr_i} \left(\frac{\partial \mathbf{u}}{\partial t} + (\mathbf{u} \cdot \nabla) \mathbf{u} \right) = -\nabla P + \mu^* \nabla^2 \mathbf{u} + \frac{d\mu^*}{dT} \nabla T \cdot (\nabla \mathbf{u} + \nabla \mathbf{u}^t) - Ra_i T \mathbf{n}, \quad (1)$$

where \mathbf{u} is the velocity field, P pressure, g the acceleration due to gravity and μ^* the dimensionless viscosity function. Superscript (t) denotes the transpose operator. The dimensionless numbers are therefore

$$Pr_i = \mu_i / \rho_0 \kappa, \quad (2a)$$

$$Ra_i = \rho_0 \alpha \Delta T_i g d^3 / \kappa \mu_i \quad (2b)$$

together with ‘viscosity’ numbers which appear in the viscosity function. For Golden Syrup, there are four of them because dimensionless viscosity is written (Appendix A)

$$\mu^* = r_i \exp \left(\frac{1}{a_i T^2 + b_i T + c_i} \right). \quad (2c)$$

For simplicity, we shall first describe our results with only one viscosity parameter, the viscosity ratio $\Delta\mu = \mu(T_b)/\mu(T_i)$, which is one particular combination of the four numbers (r_i, a_i, b_i, c_i). We shall then use all parameters in a dimensional analysis.

The experiments are listed in table 2, and cover a range of viscosity contrast of 10^0 – 10^6 . They span a larger range of dynamics than might be suspected. In an experiment, the temperature difference across the upper boundary layer decreases, and the interior viscosity increases. We may calculate values of the Rayleigh number using the instantaneous values of temperature difference and interior viscosity. Over the duration of an experiment, the ‘instantaneous’ Rayleigh number typically decreases by a factor of 20. The range of effective Rayleigh numbers for this study is from about 10^6 to 10^8 . As shown in Appendix B, in these conditions, boundary-layer instabilities are

No.	Fluid	$\Delta\mu_1$	Ra_1	Pr_1	ΔT_1 (°C)	T_c (°C)
4.00	S	1.5	1.8×10^7	8×10^3	20.70	19.25
4.01	S	1.5	1.4×10^7	9×10^3	20.10	10.10
4.02	S	2.1	3.6×10^7	8×10^3	37.80	7.20
4.03	S	1.5	3.9×10^7	7×10^3	40.95	4.10
4.13	GS	2.59×10^3	1.9×10^7	4.7×10^3	54.10	0.80
4.14	GS	9.76×10^2	1.7×10^7	4.8×10^3	49.65	5.05
4.15	GS	8.08×10^2	1.7×10^7	4.8×10^3	48.80	5.90
4.16	GS	5.50×10^4	2.0×10^7	4.8×10^3	64.25	-10.85
4.18	GS	1.18×10^2	1.7×10^7	4.0×10^3	39.60	17.00
4.19	GS	2.60×10^1	1.6×10^7	4.0×10^3	30.65	28.35
4.21	GSD	1.17×10^1	1.4×10^8	7.3×10^2	30.81	20.56
4.23	GSD	6.40	5.2×10^7	1.4×10^3	21.47	20.12
4.24	GSD	3.70×10^1	1.9×10^8	7.3×10^2	41.00	10.35
4.25	GSD	5.60×10^2	2.7×10^8	7.3×10^2	58.75	-7.52
4.26	GSD	6.50	1.8×10^7	3.5×10^3	18.29	11.64
4.28	GSD	4.95×10^2	1.7×10^7	7.1×10^3	40.00	-17.60
4.29	GSD	4.30×10^3	2.9×10^8	7.2×10^2	68.70	-17.14
4.31	GSD	8.09×10^2	1.7×10^7	7.1×10^3	41.55	-19.85
4.32	GSD	1.12×10^1	7.5×10^8	2.1×10^3	19.62	1.62
4.33	GSD	6.20	2.5×10^7	2.3×10^3	19.27	15.62
4.40	GS	1.85×10^2	1.4×10^7	4.8×10^3	41.16	13.44
4.41	GS	9.60×10^5	2.5×10^7	4.8×10^3	73.20	-18.77
4.43	GS	1.30×10^5	2.4×10^7	4.8×10^3	67.80	-13.28
4.44	GS	9.30×10^3	2.1×10^7	4.8×10^3	58.97	-4.42

TABLE 2. List of experiments: S denotes silicone oil, GS Golden Syrup and DGS Golden Syrup diluted with water

Type	Depths (in cm)
Thermocouple	0 (copper plate) 0.37, 1.12, 2.22, 2.92, 9.92, 20.12 (bottom plate)
Platinum wire	0.34, 0.54, 1.04, 1.54, 2.07, 3.07, 4.07, 6.07, 8.10, 10.10, 12.10, 14.14, 16.12, 17.03, 18.12, 18.60, 19.12, 19.64, 19.84

TABLE 3. Depth coordinates of temperature measurement devices. These coordinates correspond to experiment no. 4.41 only, as there were slight changes of positions between experiments, due to changes of the frame and spring positions, and to thickness variations of the sealant at the top and bottom of the tank

determined primarily by local conditions. Explicit use of this will be made in the scaling analysis.

2.3. Temperature measurements

Two systems were used (figure 1). A set of 19 very thin platinum wires (0.2 mm diameter) were stretched horizontally across the tank in a wedge configuration. The wires were attached to springs which were themselves attached to insulating Teflon screws placed through a thin metal frame. With this set-up, the wires are not affected by any thermal expansion or contraction of the holding frame. They allow the determination of the horizontally averaged temperature. At the Rayleigh number of 10^7 , we had between four and five data points in the upper boundary layer. A set of five thermocouples was also used to measure local temperature at selected locations, with four of them located near the upper boundary. Table 3 lists the coordinates of all these probes. Thermocouples were placed in the Styrofoam walls surrounding the tank,

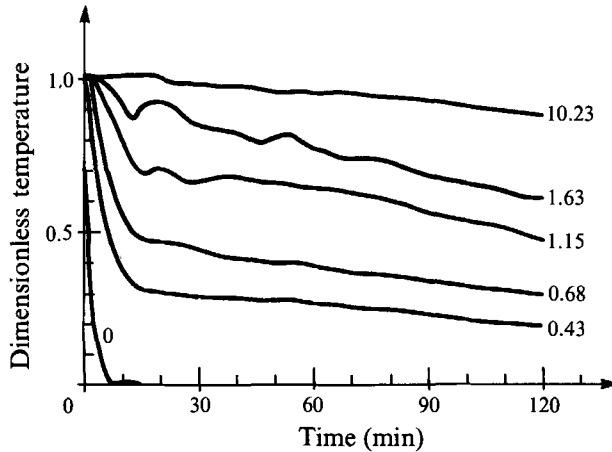


FIGURE 3. The average temperature of the platinum wires as a function of time in experiment 4.16 (see table 2 for conditions). The depths of the wires are given in cm on each curve. The curve labelled 0 corresponds to the copper plate at the top of the tank: note that its temperature drops to its final steady-state value in about 6 minutes, before the onset of convection at $t_c = 10$ minutes.

in the lower and upper plates and in the laboratory. All temperatures were read every 30 s through a scanning voltmeter connected to a computer.

The probes were designed to be much smaller than the dimensions of the convective plumes, typically by at least an order of magnitude, so that they did not perturb the flow significantly. To establish that they do not give erroneous readings, we proceeded as follows (Davaille 1991). We first used two different holding frames with different geometrical arrangements and spacing and verified that both gave similar readings in similar experiments. We also compared the temperature data obtained with the wires and the thermocouples, which are in different locations and represent different perturbations to the flow (figure 1). In an experiment, temperatures are steadily evolving with time as the fluid layer cools, but we expect 'quasi-ergodic' conditions, such that time and spatial averages are locally equivalent. The smoothed time series from the thermocouples gave the same temperature values as the wires at the same depths. Another test was that, in the limit of small viscosity variations, we obtained the same heat flux values as previous authors (see §4.3 below). Special care was taken to provide independent verification of the results and to evaluate the errors involved, as made clear in the following section.

The platinum wires are located to within ± 0.2 mm and give temperature values with an accuracy of ± 0.1 °C. Measurements made with these wires are shown in figure 3. Large fluctuations are apparent in the initial stages of convection because the first instability involves the whole boundary layer simultaneously. Later in the experiment, convective instabilities are not synchronous anymore. Each wire achieves a nearly random sampling of the various stages of an instability, and its average temperature evolves smoothly as time proceeds. Weak fluctuations remain and have been smoothed with a moving average.

The thermocouple probes have a 2 mm diameter and give temperature values at depths known to within ± 1 mm with an accuracy of ± 0.025 °C. Their response time is about 2 s, which is much smaller than the period of fluctuations in these experiments (typically several minutes). The measurements exhibit large fluctuations which record the passage of plumes (figure 4). Temperature fluctuations were determined by

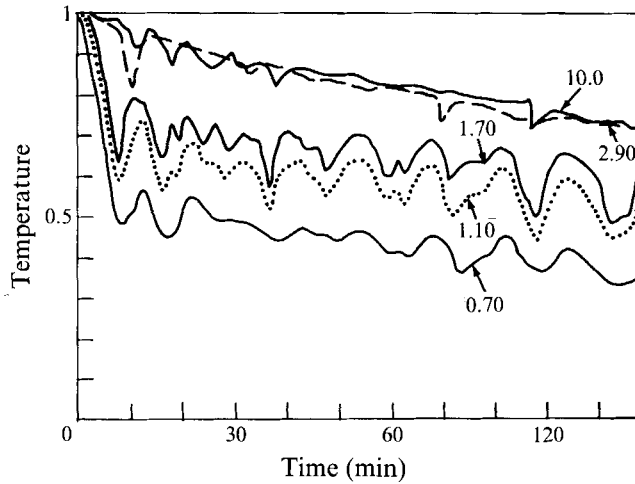


FIGURE 4. The time evolution of the local temperature measured by thermocouples in experiment 4.19. Depths are given in cm. Fluctuations due to cold plumes are visible. The period of the fluctuations increases from about 7 minutes at the onset of convection to 15 minutes after 2 h.

removing from the readings the long-term trend obtained from the smoothed time series.

3. Heat flux and boundary-layer structure

The data were interpreted with the help of the heat equation. Local temperature is decomposed into its horizontal average, $\bar{T}(z, t)$, and a fluctuation, θ . The horizontal average of the heat equation is

$$\rho_0 C_p \left(\frac{\partial \bar{T}}{\partial t} + \frac{\partial \bar{w}\theta}{\partial z} \right) = \frac{\partial}{\partial z} \left(k \frac{\partial \bar{T}}{\partial z} \right). \quad (3)$$

3.1. Heat flux determination

The heat flux through the upper boundary of the fluid layer is

$$Q_s(t) = -k_b \frac{\partial \bar{T}}{\partial z}(0, t), \quad (4)$$

where k_b is thermal conductivity at the upper boundary temperature, T_b . For the reduced range of temperature variations in the boundary layer, it is possible to neglect the temperature dependence of conductivity. In this case, (3) implies that

$$\frac{\partial^2 \bar{T}}{\partial z^2}(0, t) = 0. \quad (5)$$

The Taylor expansion of the horizontally averaged temperature near $z = 0$ can thus be written as follows:

$$\bar{T}(z, t) = \bar{T}(0, t) + z \frac{\partial \bar{T}}{\partial z}(0, t) + \frac{z^3}{3!} \frac{\partial^3 \bar{T}}{\partial z^3}(0, t) + O(z^4). \quad (6)$$

In the boundary layer, we use two and three measurements to define first-degree and third-degree polynomial approximations of the temperature profile. This gives two independent estimates of the temperature gradient at $z = 0$. We expect the two-point estimate to be slightly smaller than the latter, owing to the neglect of the curvature

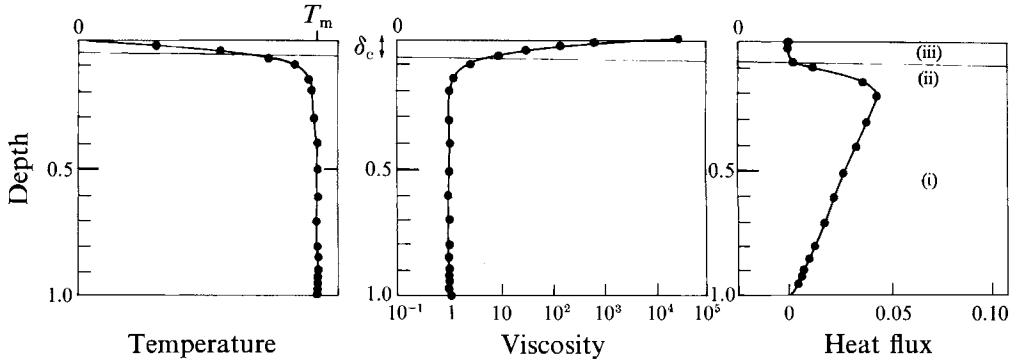


FIGURE 5. Vertical profiles of horizontally averaged temperature, viscosity and convective heat flux for fully developed convection in experiment 4.41. Viscosity and heat flux have been made dimensionless using viscosity at the interior temperature and the local heat flux scale Q_b (equation (12)) respectively. The fluid layer can be divided in (i) the well-mixed interior, (ii) the unstable part of the thermal boundary layer and (iii) a stagnant lid.

of the temperature profile. Further, we expect that the difference between the two decreases as a function of viscosity contrast, when the stagnant lid increases in thickness (Davaille 1991). Indeed, at the highest viscosity contrast when the lid is thickest, the two heat flux estimates were identical. We estimate that the heat flux values are known to better than $\pm 5\%$. An additional check on the heat flux determination is provided below.

Integrating (3) between depths $z = 0$ and z , we obtain

$$\rho_0 C_p \{\overline{w\theta}(z) - \overline{w\theta}(0)\} = k \frac{\partial \bar{T}}{\partial z}(z, t) - k \frac{\partial \bar{T}}{\partial z}(0, t) - \int_0^z \rho_0 C_p \frac{\partial \bar{T}}{\partial t}(z, t) dz. \quad (7)$$

At the upper rigid boundary, $\rho_0 C_p \overline{w\theta}(0) = 0$. Equation (7) reduces to an equation for the convective heat flux. At each time, a piecewise cubic-spline interpolation of the 21 temperature measurements is carried out which allows the determination of spatial derivatives. The same procedure is followed for the time series at each depth, and this yields the time derivative of temperature. These values are then used again in a cubic-splines interpolation scheme to calculate the time integral. We calculate the convective heat flux at each depth z starting from $z = 0$ where it is set to zero by definition. From the error values in all variables involved, we estimate the error in heat flux values to be smaller than 5%. As shown in figure 5, the convective heat flux decreases as z tends to 1. By definition, it must vanish at $z = 1$ (the tank bottom). Using the calculated value at $z = 1$, we obtain a ‘closure’ error by dividing it by the maximum value in the layer. In all cases, this ratio was found to be less than 6%. This is close to the error estimate obtained by considering the uncertainties on the various variables, and hence indicates that heat gains from the tank walls are small.

3.2. The stagnant lid thickness

By definition, in a stagnant lid, heat transfer occurs by conduction only. Figure 5 shows the vertical profile of convective heat flux, which is indeed zero near the upper boundary. To calculate the lid thickness (figure 6), we draw the tangent through the inflexion point and determine the intersection with the vertical axis ($\overline{w\theta} = 0$). The inflexion point is difficult to determine, however the tangent through it is well defined. An alternative way to define the bottom of the lid would be at depth z where the convective heat flux drops to some fixed fraction of the maximum value in the layer.

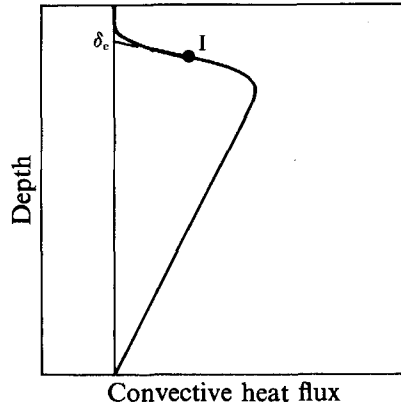


FIGURE 6. Sketch showing the vertical profile of the convective heat flux and the method used to calculate the thickness of the stagnant lid. The tangent through the inflexion point (I) intersects the zero-heat-flux axis at some depth δ_c . This depth goes to zero as the viscosity contrast goes to one, i.e. when approaching the constant-viscosity case.

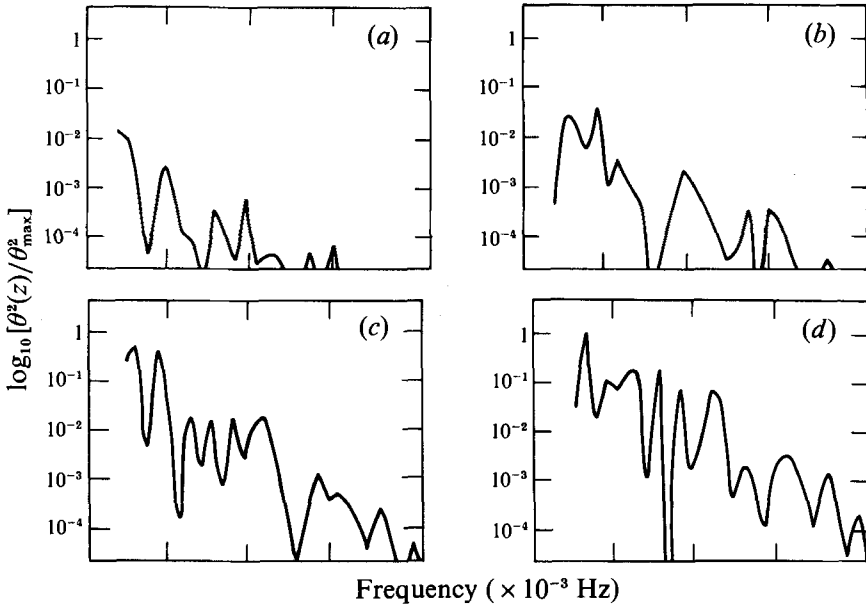


FIGURE 7. Spectrum of temperature fluctuations for experiment 4.41 at four depths near the top of the fluid layer (a) $z = 0.37$ cm, (b) $z = 1.2$ cm, (c) $z = 2.22$ cm, (d) $z = 2.92$ cm. Fluctuations have been made dimensionless with the largest value recorded. The amplitude of fluctuations decreases as depth increases, and the magnitude of this decrease is much larger at high frequency.

However, this is not satisfactory because, in the case of constant viscosity, it does not yield a zero lid thickness. With the inflexion point method, the constant-viscosity case is indeed associated with no lid.

For verification, we used a second method. The fluid layer is decomposed into a stagnant region of thickness δ_c , below which temperature fluctuations occur due to convection. These fluctuations propagate through the lid by diffusion and are damped. We consider the heat conduction problem in a layer of constant thickness δ_c with the following boundary conditions:

$$\theta(0, t) = 0 \quad \text{and} \quad \theta(\delta_c, t) = \sin(\omega t). \quad (8)$$

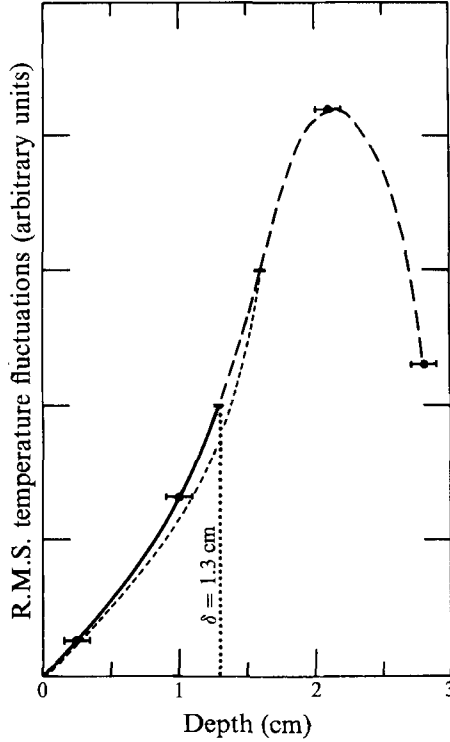


FIGURE 8. R.M.S. temperature fluctuation as a function of depth in experiment 4.41. Dots show the data points, with the maximum error in depth location. The solid and dashed curves are the theoretical response for 1.3 cm and 1.6 cm-thick lids respectively. The long-dashed curve is a fit to the data.

The solution is (Carslaw & Jaeger 1959)

$$\theta(z, t) = A \sin(\omega t + \Phi) + 2\pi\kappa \sum_{n=1}^{\infty} (-1)^{n+1} \frac{n\omega\delta_c^2}{n^4\kappa^4\pi^4 + \omega\delta_c^2} \sin\left(\frac{n\pi z}{\delta_c}\right) \exp\left(-\frac{\kappa n^2\pi^2 t}{\delta_c^2}\right), \quad (9a)$$

where

$$A = \left[\frac{\cosh(2\beta z) - \cos(2\beta z)}{\cosh(2\beta\delta_c) - \cos(2\beta\delta_c)} \right]^{\frac{1}{2}}, \quad (9b)$$

$$\Phi = \arg\left(\frac{\sinh\{\beta z(1+i)\}}{\sinh\{\beta\delta_c(1+i)\}}\right), \quad \beta = \left(\frac{\omega}{2\kappa}\right)^{\frac{1}{2}}. \quad (9c, d)$$

This equation includes an initial transient which becomes negligible rapidly. The remainder is the damped periodic response of the lid to temperature fluctuations from the convecting interior. Damping factor A depends on the lid thickness and the frequency of the fluctuation.

Using the thermocouples, we determine the spectrum of temperature fluctuations over a total time of 128 minutes. The time series at each depth, $\theta(t)$, is tapered using a Hanning window (Bloomfield 1976) and its Fourier transform is calculated using an FFT program (figure 7). For each frequency, the data are then constrained to lie between two theoretical predictions (figure 8). With this method, we determine the lid thickness with an accuracy of about 1 mm. Obviously, thicknesses smaller than the depth of the first thermocouple (0.37 cm) cannot be resolved. One drawback is that the

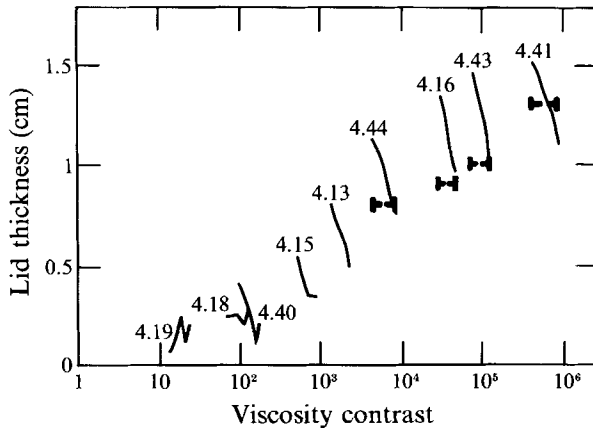


FIGURE 9. Lid thickness as a function of viscosity contrast. The numbers are experiment numbers from table 2. The continuous curves are obtained with the heat flux method of figure 5. The thick marks correspond to the smallest lid thickness as determined from the damping of temperature fluctuations.

method only gives the smallest lid thickness over the total duration of the time series. With these limitations in mind, we find excellent agreement between the two methods of determining the lid thickness (figure 9).

4. The characteristics of convection

4.1. The onset of convection

The onset of instability is defined as the time at which the temperature deviates from the initial cooling trend by $\Delta T/10^2$ (figure 10). In one experiment, the insulating material was removed and photographs were taken (figure 11), showing that convective motions take the form of downgoing plumes generated at the upper boundary. In the case of constant viscosity, the onset of instability is very sharp (figure 10*a*) and is recorded simultaneously at all depths in the boundary layer. Below the boundary layer, the temperature stays constant until the arrival of convective plumes. The variable-viscosity case is markedly different (figure 10*b*). The onset of convection is characterized by a smaller temperature deviation, indicating that the instability involves only part of the boundary layer. Further, the deviation does not occur at the same time everywhere in the boundary layer. In the example of figure 10(*b*), the $z = 0.34$ point sees its first temperature perturbation five minutes later than the critical time. The reason for this is that instability affects the upper part of the boundary layer indirectly, through conductive heat transport.

With our method, the critical time for the onset of instability is determined with an error of ± 15 s, i.e. between two successive temperature scans. The values obtained were made dimensionless using the local timescale for boundary-layer instabilities:

$$\tau_b = \frac{d^2}{\kappa} Ra_i^{-\frac{2}{3}}. \quad (10)$$

The dimensionless critical time increases as a function of viscosity contrast (figure 12). The data exhibit some scatter, which is expected as instability develops out of perturbations which may not be identical in all experiments. In constant-viscosity fluids, the onset time has a standard deviation of about 10% (Blair & Quinn 1969;

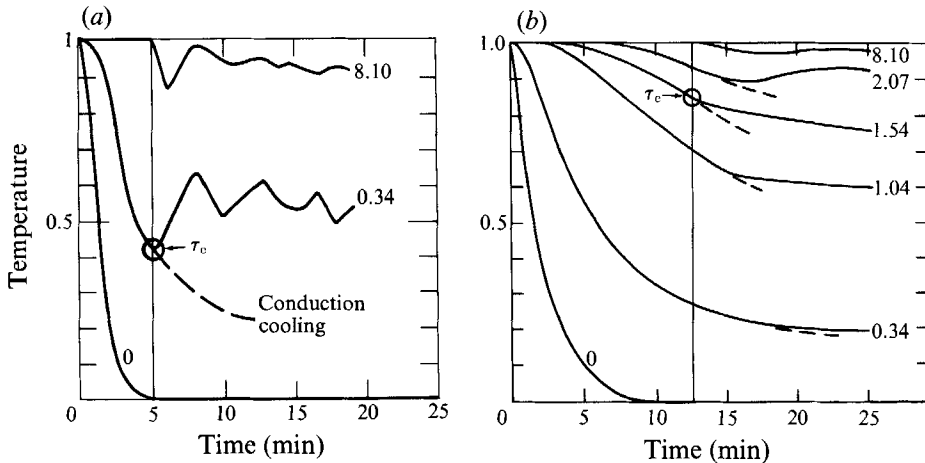


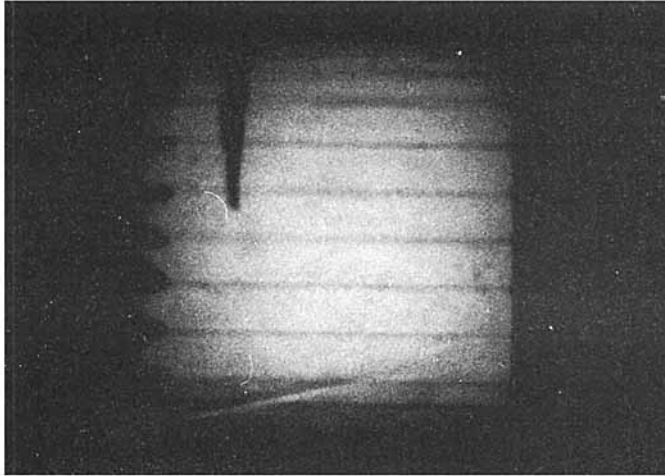
FIGURE 10. Time-evolution of the horizontally averaged temperature across the onset of convective instability. Numbers correspond to depth in cm. (a) Low viscosity contrast (experiment no. 4.00). Initially, the temperature data follow exactly the conduction solution. At $t = 5$ minutes, a sharp temperature increase occurs at $z = 0.34$ cm as the cold boundary layer detaches. At $z = 8.1$ cm, the first thermal perturbation reflects the passage of cold plumes: it occurs slightly later and is one of temperature decrease. (b) Large viscosity contrast (experiment no. 4.41). The first departure from the conduction evolution occurs at $t = 12.5$ minutes and $z = 1.54$ cm. Deeper fluid regions ($z = 2.07$) record smaller temperature increases, as the instability involves smaller temperature contrasts. Shallower fluid regions exhibit smaller perturbations at later times, for example at $t = 17$ minutes at $z = 0.34$, contrary to what would happen if they were involved in the instability.

Jhaveri & Homsy 1982). The onset time shows no appreciable variation for viscosity contrasts below a value of about 10, and starts increasing at larger values of the viscosity contrast. These data can be used to determine a criterion for the onset of instability, but this is outside the scope of the present paper.

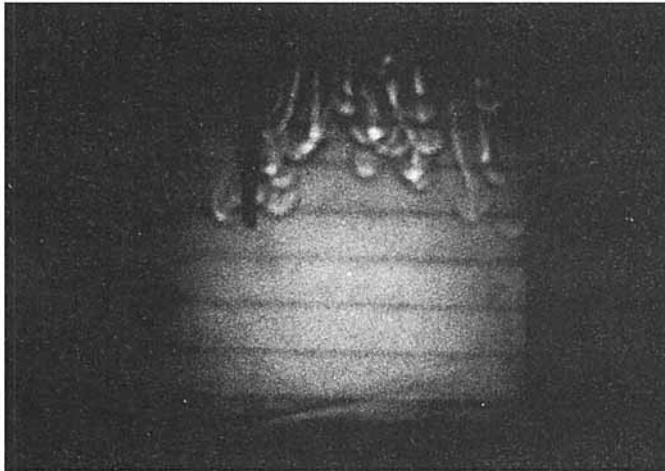
4.2. Convection at the onset time and in the fully developed regime

The characteristics of convection at the onset of instability are not representative of those of fully developed convection. In particular, the temperature difference involved in the instabilities is much smaller near the onset time than at later times. This is important because several studies have attempted to predict the features of finite-amplitude convection from marginal stability analyses (e.g. Smith 1988).

Figure 13 shows vertical temperature profiles at several times close to the critical time for experiment no. 4.13. Until this time, the data follow exactly the conduction solution. At the critical time, the temperature profile differs from the conduction solution. This difference is restricted to the lower part of the boundary layer, showing that convective breakdown does not affect the uppermost fluid regions where viscosity is largest. The viscosity contrast across the unstable part of the boundary layer is between 2 and 3 in all experiments, in agreement with the theoretical results of Smith (1988). At the later time of 12 minutes, the temperature profile has developed a reversal which is not seen in the previous profiles. This feature is due to the mechanism of the instability: the lower part of the boundary layer has detached and has been replaced by hotter fluid, which leads to an S-shaped temperature profile. This profile is then smoothed out by thermal diffusion. After 20 minutes, the temperature profile has the same complex shape, but the stagnant lid is thinner than before. We interpret this as due to the local viscosity profile, which determines the characteristics of the instability,



(a)



(b)

FIGURE 11. Shadowgraph pictures for experiment 4.29. (a) 15 s after the onset of instability as defined from the temperature recordings: no motion is visible in the interior. (b) 45 s after the onset of instability: plumes have detached from the upper boundary layer.

as shown by Jaupart & Parsons (1985). Just at the critical time, the temperature gradient increases rapidly towards the top of the fluid layer, implying a sharp increase of viscosity which does not favour penetration. As convection develops, heat is brought into the boundary layer and the temperature profile is less steep, implying a more gradual viscosity increase. This allows the instability to involve a larger thickness of fluid, which results in a thinner lid. At later times, the fluid layer cools and becomes more viscous, and the lid gradually thickens (figure 13).

The stagnant lid is thicker for larger values of viscosity contrast (figure 9). For each individual experiment, the lid thickness increases with time, save for an initial transient following the onset of instability. The variation of lid thickness for each experiment does not follow the general trend of all experiments considered together, which indicates that the viscosity contrast alone is not sufficient to describe the data.

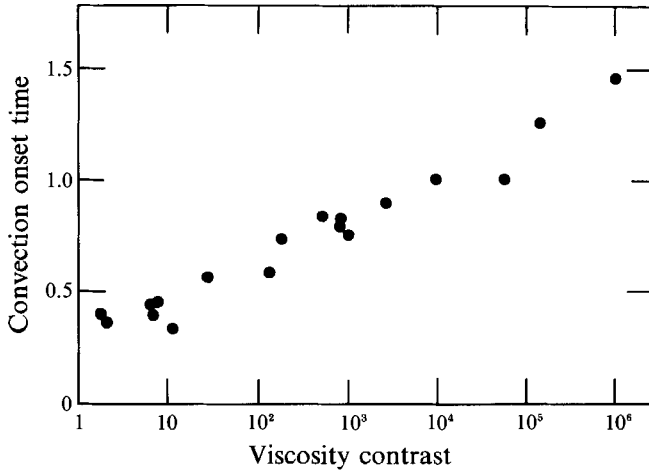


FIGURE 12. The critical time for the onset of convection as a function of viscosity contrast, made dimensionless using the local scale τ_b , (equation (10)). There is no appreciable variation for viscosity contrasts less than 10.

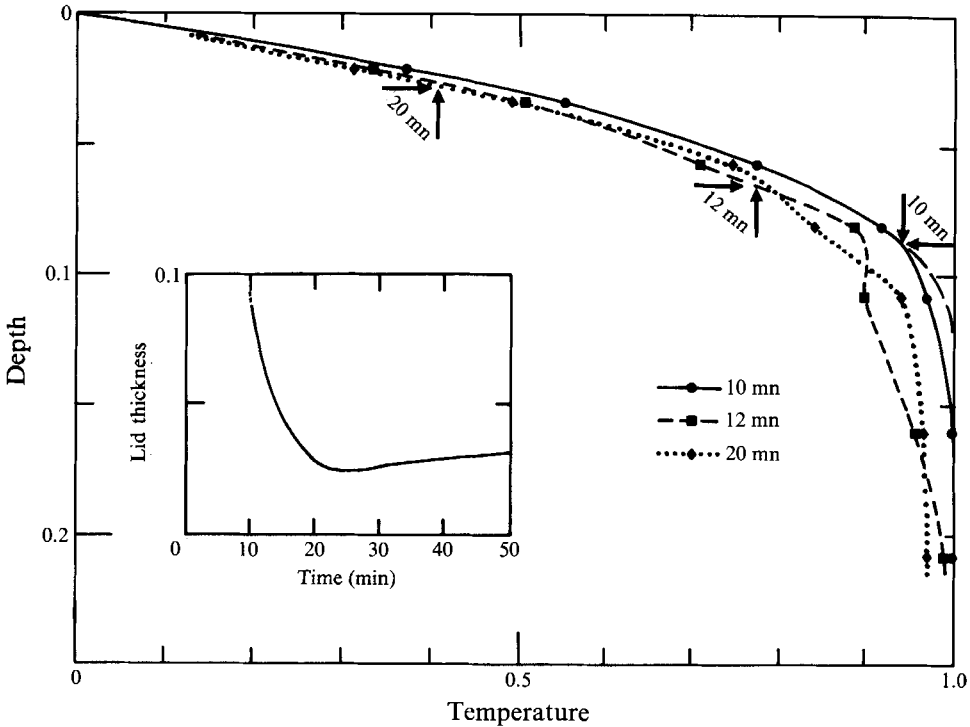


FIGURE 13. Vertical profiles of the horizontally averaged temperature in experiment 4.13. Just after the critical time ($t_c = 9.5$ minutes), temperatures differ from the conduction profile (long dashes) only in the lower parts of the boundary layer. At later times, the distorted temperature profiles reflect the response of a conductive lid overlying an unstable layer undergoing intermittent breakdown. The arrows give the lid positions. The inset shows how the lid thickness evolves with time.

4.3. Thermal structure and evolution of the convecting layer

Shadowgraph observations do not provide any evidence for any large-scale circulation over the dimensions of the tank. Plume generation is often repeated at the same location, which has also been observed in experiments with small viscosity variations

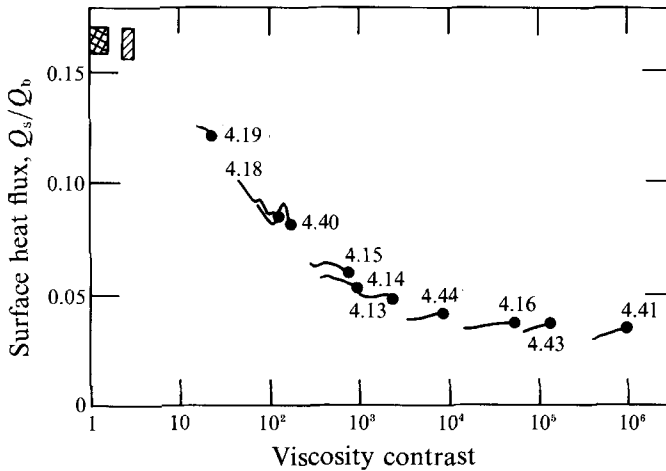


FIGURE 14. Heat flux through the upper boundary, made dimensionless with local scale (12), as a function of viscosity contrast. The experiment numbers are from table 2. The boxes shows values for weak viscosity variations with silicone oil and diluted Golden Syrup, which are less accurate. In each experiment, the dot represents the initial value at the onset of convection.

(Sparrow, Husar & Goldstein 1970; Asaeda & Watanabe 1989). One explanation may be that an instability induces temperature and hence viscosity fluctuations in the stagnant lid, which act as a 'nucleation' site for the next instability. The phenomenon is not due to the presence of temperature probes, as shown by the fact that the plume positions do change during an experiment and from one experiment to the next.

The fluid layer can be separated into three regions (figure 5): the stagnant lid, the unstable part of boundary layer, and the well-mixed interior. Figure 4 shows the evolution of temperature as a function of time in an experiment with moderate viscosity contrast (no. 4.19). Temperature fluctuations take the form of negative spikes which record the passage of cold plumes. Because of the large layer depth, the interior temperature evolves on a timescale which is much longer than the intermittency. Thus, each breakdown of the boundary layer can be thought of as occurring in a steady background temperature field. Figure 8 shows the amplitude of temperature fluctuations at large viscosity contrast. Temperature fluctuations are maximum near the bottom of the unstable boundary layer, which is consistent with the mechanism of intermittent plume release.

In the well-mixed interior, the magnitude of temperature fluctuations is considerably reduced, the horizontally averaged temperature is uniform and the convective heat flux exhibits a linear decrease with depth (figure 5). Let us denote the horizontally averaged temperature of the well-mixed layer by $T_m(t)$. The heat equation (3) therefore reduces to

$$\rho_0 C_p \left(\frac{dT_m}{dt} + \frac{\partial \bar{w}\theta}{\partial z} \right) = 0, \quad (11)$$

which shows that the convective heat flux has a constant vertical derivative.

Figure 14 shows measurements of the surface heat flux made dimensionless with the following local scale:

$$Q_b = k_m \left(\frac{\alpha g}{\kappa \nu_m} \right)^{\frac{1}{3}} \Delta T_m^{\frac{4}{3}}, \quad (12)$$

where k_m is thermal conductivity calculated at the interior temperature T_m , and

$\Delta T_m = T_m - T_b$, the total temperature difference across the boundary layer. The dimensionless heat flux decreases as the viscosity contrast increases, reflecting the fact that an increasingly large part of the thermal boundary layer does not participate in convection (figure 14). At viscosity contrasts smaller than about 5, heat flux values do not exhibit appreciable differences, in agreement with Booker (1976). These determinations are effected by larger error levels than those for pure Golden Syrup. The values are between 0.16 and 0.17, and agree with earlier determinations. Townsend (1959, 1964) and Deardorff, Willis & Lilly (1969) proposed values of 0.19 and 0.20 ± 0.2 respectively for water, and the more precise measurements of Katsaros *et al.* (1977) led to a value of 0.156.

5. Local dimensional analysis

5.1. Local heat flux and temperature scales

The fluid layer evolves on a timescale which is much larger than the intermittency of convective breakdown (figure 4). This reflects the basic fact that a thin boundary layer is acting to cool a much larger body of fluid. We argue that, at each time, the dynamics of instability depend only on the instantaneous state of the upper boundary layer and hence can be characterized by the instantaneous values of the parameters, i.e.

$$\Delta T_m = T_m - T_b, \quad \nu_m = \nu(T_m). \quad (13)$$

This approach would not be valid in the study of the large-scale velocity field in the layer interior because it evolves on a longer timescale. The following analysis is restricted to boundary-layer processes and its validity will be verified by its implications (see (18) below).

We use the dimensional analysis of §2 based on external scales for the variables. For large Prandtl number, the dimensionless heat flux may be written as follows:

$$Q^* = \frac{Q_s}{-k_m \Delta T_m / d} = F_1(Ra_m, r_m, a_m, b_m, c_m), \quad (14)$$

where all dimensionless numbers are defined as in §2 and calculated using the local values (13). Convective instabilities are determined solely by local conditions in the boundary layer, and hence are independent of the layer depth d . This determines the dependence of Q^* on Ra_m . The surface heat flux, Q_s , can now be written as

$$Q_s = -k_m \left(\frac{\alpha g}{\kappa \nu_m} \right)^{\frac{1}{3}} \Delta T_m^{\frac{4}{3}} F_2(r_m, a_m, b_m, c_m). \quad (15)$$

We next argue that this heat flux does not depend on the total temperature difference ΔT_m because part of the boundary layer remains stable. The driving temperature difference depends only on local conditions in the unstable boundary layer. Accordingly, we write heat flux as

$$Q_s = -k_m \left(\frac{\alpha g}{\kappa \nu_m} \right)^{\frac{1}{3}} \Delta T_c^{\frac{4}{3}}, \quad (16)$$

where the local temperature difference ΔT_c is given by

$$\Delta T_c = \Delta T_m (F_2(r_m, a_m, b_m, c_m))^{\frac{3}{4}}. \quad (17)$$

The reasoning predicts that this temperature difference depends only on the viscosity profile in the unstable boundary layer, at temperatures close to the interior temperature

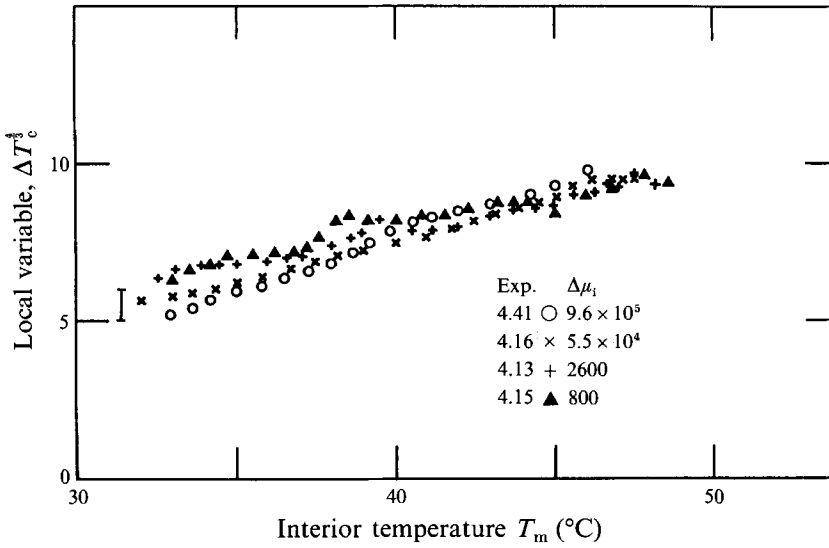


FIGURE 15. Plot of $\Delta T_c^{\frac{4}{3}}$ from equation (18) as a function of viscosity contrast for four representative experiments spanning three orders of magnitude of viscosity contrast. The vertical bar shows the experimental error.

T_m . For a given viscosity function, this difference should therefore depend only on the interior temperature T_m . We test this by writing

$$\Delta T_c^{\frac{4}{3}} = \frac{Q_s}{-k_m(\alpha g/\kappa\nu_m)^{\frac{1}{3}}}, \tag{18}$$

which is calculated from the experimental data and shown as a function of the interior temperature T_m in figure 15. The scaling argument predicts that the values should collapse onto a single curve, which is verified within the accuracy of the measurements. This provides a justification for our starting assumption.

5.2. The ‘viscous’ temperature scale

As indicated by (17), the driving temperature difference depends on several variables describing the viscosity function. However, instabilities are confined to a region where viscosity variations are reduced, and we propose to approximate locally the viscosity function by an exponential. In this case, a ‘viscous’ temperature scale may be defined as

$$\Delta T_v = -\frac{\mu(T_m)}{(d\mu/dT)(T_m)}. \tag{19}$$

Using the full viscosity function (equation (2c)), it can be seen that this definition is indeed of the form (17) required by the dimensional analysis:

$$\Delta T_v = \frac{(a_m T_m^* + b_m T_m^* + c_m)^2}{-2a_m T_m^* - b_m} \Delta T_m. \tag{20}$$

Using this temperature scale, we define the corresponding heat flux scale Q_v with an equation of the form (12):

$$Q_v = k_m \left(\frac{\alpha g}{\kappa\nu_m} \right)^{\frac{1}{3}} \Delta T_v^{\frac{4}{3}}. \tag{21a}$$

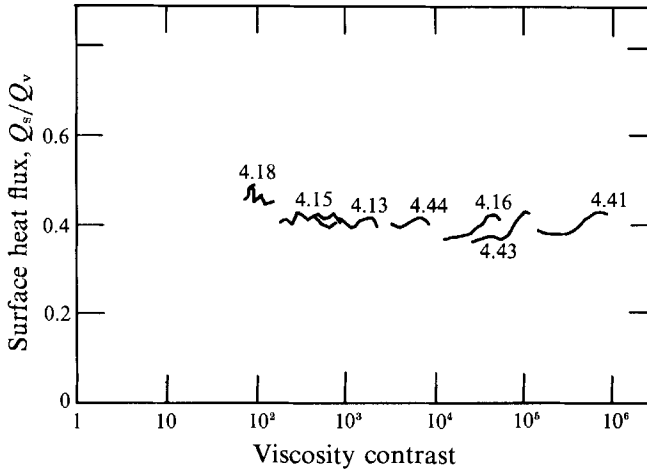


FIGURE 16. Heat flux made dimensionless using the ‘viscous’ scales (equations (19) and (21a)), as a function of viscosity contrast for all experiments with viscosity contrasts greater than 10^2 . The experimental error is $\pm 5\%$.

Heat flux determinations made dimensionless with this new scale are shown in figure 16. The resulting values can be considered identical given the magnitude of measurement errors. This indicates that the temperature difference ΔT_c in (17) is indeed proportional to the viscous temperature scale. We conclude that, at high viscosity contrast, the heat flux is given by the following equation:

$$Q_s = -Ck_m \left(\frac{\alpha g}{\kappa \nu_m} \right)^{\frac{1}{3}} \Delta T_v^{\frac{4}{3}}. \quad (21b)$$

Depending on the conductivity values for Golden Syrup at low temperatures (Appendix A), constant C takes different values: 0.41 ± 0.03 for Wray’s determinations and 0.47 ± 0.03 for our own.

Another understanding of the ‘viscous’ temperature scale can be obtained by going back to the momentum equation (1). This equation contains two dimensionless variables: viscosity and the derivative of viscosity with temperature. One might argue that both variables must take values of order 1 in the unstable boundary layer. Indeed, we have shown experimentally that the first variable never exceeds a value of about 10. The second variable is the dimensionless derivative of viscosity. If we use the external temperature scale, ΔT_i , it takes a representative value of $\Delta T_i/\Delta T_v$, which can be made arbitrarily high if ΔT_i is increased. This is clearly not appropriate and shows that temperature must be rescaled with ΔT_v .

5.3. The ‘lid’ model

The stagnant lid passively transports the heat brought from below by convection, and displaces the rigid boundary downwards (Nataf & Richter 1982). According to the phenomenological model of intermittent plume release, the magnitude of temperature fluctuations in the convecting fluid must be proportional to the temperature difference across the unstable boundary layer (Townsend 1959; Howard 1964). Comparison with constant-viscosity experiments is not straightforward. There is a steady evolution of convection conditions as the fluid layer cools, and hence the timeseries does not sample all the possible fluctuations. We proceeded as follows. We took the largest fluctuations

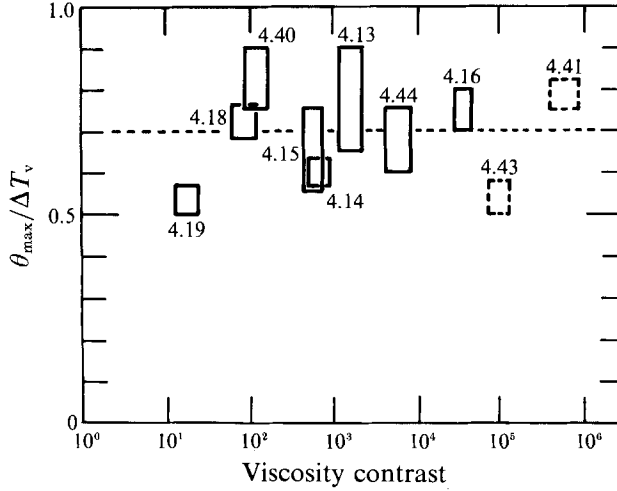


FIGURE 17. The maximum amplitude of temperature fluctuations in the boundary layer, θ_{\max} , as a function of the viscous temperature scale ΔT_v . The domain for each experiment is shown as a box: boxes with dashed edges correspond to experiments with poor sampling in the boundary layer. The dashed horizontal line corresponds to the average value for all experiments.

recorded, and estimated their maximum amplitude in the boundary layer, which we call θ_{\max} . We compare this to the value of ΔT_v at the same time (figure 17). The data exhibit some scatter which can be attributed to the insufficient sampling achieved, but which is a small fraction of the total temperature difference across the boundary layer, ΔT_m . The best-fit relationship between θ_{\max} and ΔT_v is

$$\theta_{\max} = 0.70 \times \Delta T_v. \quad (22)$$

To determine the temperature difference across the unstable boundary layer, which we call ΔT_e , we have used two methods which gave the same result. One is to measure it directly from the temperature profiles below the stagnant lid. The other is to refer to the heat flux equation. In the unstable part of the boundary layer, viscosity contrasts never exceed a value of 15 and, in these conditions, heat flux should be given by the usual equation:

$$Q_s = -C^* k_m \left(\frac{\alpha g}{\kappa \nu_m} \right)^{\frac{1}{3}} \Delta T_e^{\frac{4}{3}}, \quad (23)$$

where C^* is a constant equal to 0.16 (Katsaros *et al.* 1977). Equating the two heat flux equations leads to

$$C^* \Delta T_e^{\frac{4}{3}} = C \Delta T_v^{\frac{4}{3}}. \quad (24)$$

For the experimentally determined values of 0.16 and 0.41 for C^* and C respectively, we find $\Delta T_e \approx 2\Delta T_v$. We thus relate the largest temperature fluctuation θ_{\max} to the temperature difference ΔT_e :

$$\theta_{\max} \approx 0.35 \times \Delta T_e. \quad (25)$$

This is close to the observations of Thomas & Townsend (1957).

Assuming a sinusoidal fluctuation with a single frequency, the corresponding r.m.s. amplitude is $0.25 \times \Delta T_e$ with Wray's conductivity values and $0.21 \times \Delta T_e$ with our own. We have only recorded the largest fluctuations, and hence these values must be

considered as upper bounds when compared to the value of 0.18 measured by Townsend (1959) and predicted by Howard (1964). Precise comparisons are unwarranted because the presence of a conducting region above a fluid layer changes the dynamics (Hurle, Jakeman & Pike 1967; Busse & Riahi 1980). The agreement can thus be considered satisfactory and validates the model of intermittent plume release.

Across the lid of thickness δ_c , the temperature difference is $(\Delta T_m - \Delta T_e)$. Thus, the surface heat flux Q_s must be

$$Q_s = -k_b \frac{\Delta T_m - \Delta T_e}{\delta_c}. \quad (26)$$

Using equation (21a), this equation is recast as one for δ_c :

$$\delta_c = \frac{1}{C} \frac{k_b}{k_m} \left\{ \frac{\Delta T_m}{\Delta T_v} - \frac{\Delta T_e}{\Delta T_v} \right\} \left\{ \frac{\alpha g \Delta T_v}{\kappa \nu_m} \right\}^{-\frac{1}{3}}. \quad (27)$$

Using the experimental values for the constant C and for the temperature ratio $(\Delta T_e/\Delta T_v)$ respectively, calculated values of the lid thickness are in excellent agreement with the independent determinations (figure 18).

5.4. Domain of validity of the analysis

The 'whole layer' mode of convection such that the whole thermal boundary layer is involved in the instability (Jaupart & Parsons 1985; Ogawa *et al.* 1991) was only observed at low viscosity contrast. In this regime, there is no detectable difference with the constant-viscosity case (figure 12). The lowest viscosity contrast for which we were able to detect the presence of a lid is about 15 (figure 9). When a stagnant lid existed, the viscosity contrast across the unstable part of the boundary layer was never smaller than 10. Thus, a necessary condition for the presence of a 'stagnant lid' is that the viscosity contrast exceeds this value. A better criterion may be obtained from the equation for the lid thickness, which has a physical solution only when the following inequality is met:

$$\frac{\Delta T_m}{\Delta T_v} > \frac{\Delta T_e}{\Delta T_v} \quad (28a)$$

or, using the value of 2 for the ratio $\Delta T_e/\Delta T_v$:

$$\Delta T_m > 2 \frac{\mu(T_m)}{(d\mu/dT)(T_m)}. \quad (28b)$$

It can be shown that this criterion has a form similar to the one proposed by Stengel *et al.* (1982) on different grounds.

The viscosity of Golden Syrup varies with temperature in a hyperexponential way (Appendix A). An important issue is to what extent our results can be applied to other fluids with different viscosity functions. As shown by the momentum equation (1), both viscosity and the derivative of viscosity play a role, and it is the balance between the two which determines the dynamics of convection. For Golden Syrup, the details of this balance are different as the thermal conditions change, because the viscosity function is not exponential. The presence of a stagnant lid implies that only a reduced range of viscosity variation exists in the actively convecting fluid, implying a weak sensitivity to the full viscosity function. The analysis shows that it is sufficient to locally approximate the viscosity profile by an exponential one but this local function changes from one experiment to the next, as the interior temperature varies. In effect, our

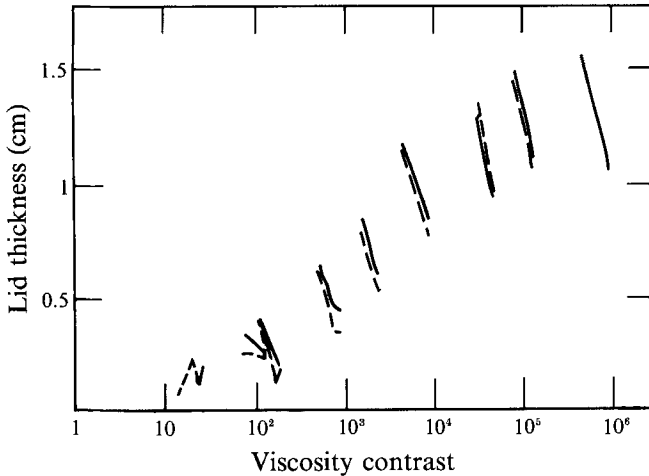


FIGURE 18. Stagnant lid thickness as a function of viscosity contrast for Golden Syrup experiments. Continuous lines are from the heat flux measurements of §3. Dashed lines correspond to the predictions of equation (27). At the highest viscosity contrast, the two sets of values cannot be distinguished from each other.

experiments span a range of local viscosity functions. This is best shown by the viscous temperature scale which is the e -folding temperature for viscosity variations. In the experiments, ΔT_v varies from 14 °C to 4 °C, i.e. by a factor of more than three, yet the scaling relationships hold for all of them. Further, measurements with diluted Golden Syrup correspond to yet another viscosity function and, although of lesser quality, are consistent with those for pure Syrup. We suggest therefore that the scaling laws derived in this paper apply to most natural fluids whose viscosity exhibits a monotonic decrease as temperature increases.

6. Conclusion

At high Rayleigh numbers and large viscosity contrast, thermal convection is such that a significant thickness of fluid remains stagnant. Convective instabilities are sensitive to the viscosity structure of the unstable boundary layer, and hence to the temperature profile. One consequence of this is that conditions at the onset of instability are not identical to those in the fully developed regime. Convection can be described using local scales in the unstable part of the boundary layer, independently of the overall temperature difference applied between the fluid interior and the upper boundary. The 'viscous' temperature scale proposed in this paper is sufficient to account for the most important characteristics of convection.

Geneviève Brandeis made preliminary experiments which helped pave the way for this investigation. Gérard Bienfait helped with the design of the apparatus and kept the laboratory in working order. We benefited from discussions with Stephen Sparks, Stephen Tait, Herbert Huppert and Neil Ribe. Three anonymous critical reviews led to a sharper and better manuscript. This study has been supported by grants from CNRS/INSU (DBT Thème 3 Instabilités contribution no.).

Appendix A. Physical properties of the working fluids

Viscosity measurements were made with a falling ball viscometer and a rotating viscometer over a range of shear rates for temperatures between $-20\text{ }^{\circ}\text{C}$ and $+70\text{ }^{\circ}\text{C}$. In these conditions, the three fluids were Newtonian with viscosity functions listed below. In all cases, measured deviations from the best-fit functions were less than 2%.

Silicone oil 47V1000

$$\mu = \mu_0 \exp(AT), \quad (\text{A } 1)$$

with $\mu_0 = 1.62\text{ Pa s}$, $A = -1.97 \times 10^{-2}\text{ }^{\circ}\text{C}^{-1}$;

Golden Syrup

$$\mu = \mu_0 \exp\left(\frac{1}{AT^2 + BT + C}\right), \quad (\text{A } 2)$$

with

$$\begin{aligned} \mu_0 &= 4.485 \times 10^{-8}\text{ Pa s}, & A &= -7.5907 \times 10^{-7}, \\ B &= 3.8968 \times 10^{-4}, & C &= 4.0130 \times 10^{-2}; \end{aligned}$$

Diluted Golden Syrup

$$\mu = \mu_0 \exp\left(\frac{1}{AT^2 + BT + C}\right), \quad (\text{A } 3)$$

with

$$\begin{aligned} \mu_0 &= 1.15 \times 10^{-5}\text{ Pa s}, & A &= -2.9146 \times 10^{-7}, \\ B &= 7.6761 \times 10^{-4}, & C &= 7.0227 \times 10^{-2}. \end{aligned}$$

In all these equations, T is in degree Celsius. The equation for Golden Syrup gives values within 5% of those quoted by White (1988).

Density was measured between temperatures of $0\text{ }^{\circ}\text{C}$ and $60\text{ }^{\circ}\text{C}$ using floating densimeters, which gave the coefficient of thermal expansion. For Golden Syrup, our values are identical to those of White (1988).

For thermal conductivity, we undertook a series of careful measurements. Wray (1978) used a coaxial cylinder apparatus, which gives conductivity values with an error of $\pm 2\%$, and investigated a temperature range of $20\text{--}60\text{ }^{\circ}\text{C}$. He gave the following relationship:

$$k(T) = 0.316 + 1.843 \times 10^{-3} \times T \text{ W m}^{-1} \text{ K}^{-1}, \text{ with } T \text{ in } ^{\circ}\text{C}. \quad (\text{A } 4a)$$

Given the error estimate and the observed conductivity variation, it is clear that this equation cannot be extrapolated with confidence. Richter *et al.* (1983) proposed another relationship which differs from this one by as much as 20% for temperatures below $0\text{ }^{\circ}\text{C}$, which are of interest here. We used a needle-probe method such that a fixed power is released over a line source buried in the liquid. This method was calibrated with solid standards, and has an accuracy of $\pm 3\%$. As in other methods, the occurrence of convection must be avoided, which was verified in two independent ways. First, we took a silicone oil with viscosity similar to that of Golden Syrup and obtained the correct conductivity value. Also, we repeated the measurements with values of the power input differing by a factor of two: any variation in the efficiency of convective heat transfer would result in different values of 'apparent' conductivity. Measurements were made in a temperature-controlled chamber at different ambient temperatures. Figure 19 summarizes the available data. Given the errors of the

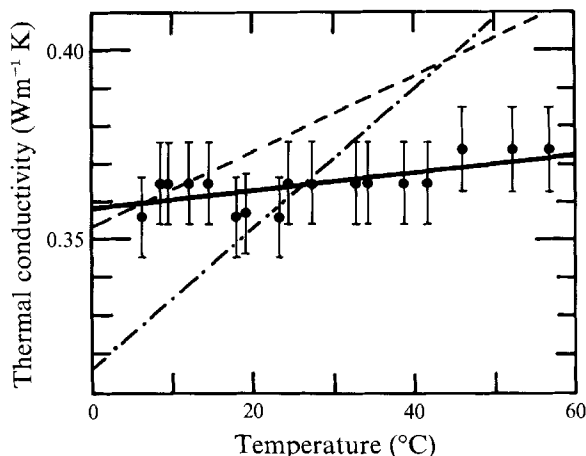


FIGURE 19. Thermal conductivity of pure Golden Syrup as a function of temperature. Dots show our measurements, and the thick line is the least-squares linear regression through the data points. Also shown are the values proposed by Wray (1978) (—) and Richter *et al.* (1983) (-·-·-).

different methods, our values are compatible with those of Wray over most of the temperature range he investigated, as well as with those of Richter *et al.* (1983). The least-squares linear regression through our data points has a positive gradient, as expected for a fluid containing water (Bird, Stewart & Lightfoot 1960):

$$k = 0.358 + 2.4 \times 10^{-4} \times T \quad \text{W m}^{-1} \text{K}^{-1}, \quad \text{with } T \text{ in } ^\circ\text{C}. \quad (\text{A } 4b)$$

This equation was adopted as an alternative to Wray's.

To obtain values of thermal diffusivity, an initially isothermal layer was heated from the top, and the temperature evolution was recorded. The heat conduction equation was integrated numerically using the true values of the upper boundary temperature $T(0, t)$ for a range of thermal diffusivity values. Calculated temperatures were compared to the measured ones. This method gives an average value of diffusivity over the temperature range considered. Our result for Golden Syrup is compatible with Wray's measurements at 20 °C (Wray 1978).

Appendix B. Dynamical regime of the experiments

At high Prandtl number, plumes are generated in the thermal boundary layer which is thinner than the momentum boundary layer. If the fluid layer is deep enough, each individual plume becomes turbulent at some distance from the boundary. Extending the analysis of Kraichnan (1962) to the variable-viscosity case, we find that this regime is not attained.

Steady-state experiments by Heslot, Castaing & Libchaber (1987) and Castaing *et al.* (1989) in helium ($0.6 < Pr < 1.7$) indicate that, at Rayleigh numbers in excess of about 10^7 , the spectrum of temperature fluctuations changes, which defines a new dynamical regime called 'hard turbulence'. Castaing *et al.* (1989) suggest that the dynamics of boundary-layer instabilities are affected by a large-scale circulation and that two lengthscales are involved: the total layer depth and the thickness of the unstable boundary layer. They propose that the Nusselt number/Rayleigh number relationship follows a $\frac{2}{7}$ power law instead of the $\frac{1}{3}$ power-law for thermal turbulence. Two additional parameters play a role: the aspect ratio of the tank and the Prandtl number. In the experiments of Castaing *et al.* (1989), the aspect ratio is unity, and it is not clear

whether it is the height or the width of the tank which affects the dynamics. According to Deardorff & Willis (1965), in air ($Pr = 0.7$) at Rayleigh numbers between 10^5 and 10^7 , it is the width effect which comes into play because it prevents the free 'mushrooming' of plumes. For large Prandtl number and large aspect ratio, there are conflicting results. In a numerical study in two dimensions, Hansen, Yuen & Kroening (1990) described a transition in flow structure at Rayleigh numbers between 10^7 and 10^8 , which they attributed to the onset of hard turbulence. However, in the experiments of Goldstein, Chiang & See (1990) at Rayleigh numbers between 10^9 and 10^{12} , the Nusselt number follows the $\frac{1}{3}$ power law.

In our experiments, the tank aspect ratio is 1.5, Prandtl numbers are always higher than 7×10^2 , and Rayleigh numbers for which heat flux determinations have been carried out are less than 2×10^7 . In transient conditions, over the duration of the recordings, it is probable that no large-scale circulation has time to develop. Interestingly, the careful study by Katsaros *et al.* (1977) in water ($Pr = 7$) was also made in transient conditions for aspect ratios between 1 and 1.5 and Rayleigh numbers between 10^6 and 10^9 , and led to a $\frac{1}{3}$ power law relationship for the Nusselt number. We thus conclude that, in our experiments, boundary-layer instabilities are determined primarily by local conditions in the unstable boundary layer.

REFERENCES

- ASAEDA, T. & WATANABE, K. 1989 The mechanism of heat transport in thermal convection at high Rayleigh number. *Phys. Fluids A* **1**, 861–867.
- BIRD, R. B., STEWART, W. E. & LIGHTFOOT, E. N. 1960 *Transport Phenomena*. Wiley.
- BLAIR, L. M. & QUINN, J. A. 1969 The onset of cellular convection in a fluid layer with time-dependent density gradients. *J. Fluid Mech.* **36**, 385–400.
- BLOOMFIELD, P. 1976 *Fourier Analysis of Time Series: An Introduction*. Wiley.
- BOOKER, J. R. 1976 Thermal convection with strongly temperature dependent viscosity. *J. Fluid Mech.* **76**, 741–754.
- BOOKER, J. R. & STENGEL, K. C. 1978 Further thoughts on convective heat transport in a variable viscosity fluid. *J. Fluid Mech.* **86**, 289–291.
- BUSSE, F. H. & FRICK, H. 1985 Square pattern convection in fluids with strongly temperature-dependent viscosity. *J. Fluid Mech.* **150**, 451–465.
- BUSSE, F. H. & RIAHI, N. 1980 Nonlinear convection in a layer with nearly insulating boundaries. *J. Fluid Mech.* **96**, 243–256.
- CARSLAW, H. S. & JAEGER, J. C. 1959 *Conduction of Heat in Solids*. Oxford University Press.
- CASTAING, B., GUNARATNE, G., HESLOT, F., KADANOF, L., LIBCHABER, A., THOMAS, S. & WU, X.-Z. 1989 Scaling of hard thermal turbulence in Rayleigh–Bénard convection. *J. Fluid Mech.* **204**, 1–30.
- CHRISTENSEN, U. & HARDER, H. 1991 3-D convection with variable viscosity. *Geophys. J. Intl* **104**, 213–226.
- DAVILLE, A. 1991 La convection thermique dans un fluide à viscosité variable. Applications à la terre. PhD thesis, Université Paris 6.
- DEARDORFF, J. W. & WILLIS, G. E. 1965 Investigation of turbulent thermal convection between horizontal plates. *J. Fluid Mech.* **28**, 675–704.
- DEARDORFF, J. W., WILLIS, G. E. & LILLY, D. K. 1969 Laboratory investigation of non-steady penetrative convection. *J. Fluid Mech.* **35**, 7–31.
- FOWLER, A. C. 1985 A simple model of convection in the terrestrial planets. *Geophys. Astrophys. Fluid Dyn.* **31**, 283–309.
- GOLDSTEIN, R. J., CHIANG, H. D. & SEE, D. L. 1990 High-Rayleigh-number convection in a horizontal enclosure. *J. Fluid Mech.* **213**, 111–126.
- HANSEN, V., YUEN, D. A. & KROENING, S. E. 1990 Transition to hard turbulence in thermal convection at infinite Prandtl number. *Phys. Fluids A* **2**, 2157–2163.

- HESLOT, F., CASTAING, B. & LIBCHABER, A. 1987 Transitions to turbulence in helium gas. *Phys. Rev. A* **36**, 5870–5873.
- HOWARD, L. N. 1964 Convection at high Rayleigh number. In *Proc. 11th Intl Congr. Applied Mechanics* (ed. H. Görtler), pp. 1109–1115. Springer, Berlin.
- HUPPERT, H. E. & SPARKS, R. S. J. 1988 Melting the roof of a chamber containing a hot, turbulently convecting fluid. *J. Fluid Mech.* **188**, 107–131.
- HUPPERT, H. E. & TURNER, J. S. 1991 Comments on ‘On convective style and vigor in sheet-like magma chambers’ by Bruce D. Marsh. *J. Petrol.* **32**, 851–854.
- HURLE, D. T. J., JAKEMAN, E. & PIKE, E. R. 1967 On the solution of the Bénard problem with boundaries of finite conductivity. *Proc. R. Soc. Lond. A* **296**, 469–475.
- JAUPART, C. & PARSONS, B. 1985 Convective instabilities in a variable viscosity fluid cooled from above. *Phys. Earth Planet. Inter.* **39**, 14–32.
- JHAVERI, B. S. & HOMSY, G. S. 1982 The onset of convection in fluid layers heated rapidly in a time-dependent manner. *J. Fluid Mech.* **114**, 251–260.
- KATSAROS, K. B., LIU, W. T., BUSINGER, J. A. & TILLMAN, J. E. 1977 Heat transport and thermal structure in the interfacial boundary layer in an open tank of water in turbulent free convection. *J. Fluid Mech.* **83**, 311–335.
- KRAICHNAN, R. H. 1962 Turbulent thermal convection at arbitrary Prandtl number. *Phys. Fluids* **5**, 1374–1389.
- MORRIS, S. & CANRIGHT, D. 1984 A boundary-layer analysis of Bénard convection in a fluid of strongly temperature-dependent viscosity. *Phys. Earth Planet. Inter.* **36**, 355–373.
- NATAF, H.-C. & RICHTER, F. M. 1982 Convection experiments in fluids with highly temperature-dependent viscosity and the thermal evolution of the planets. *Phys. Earth Planet. Inter.* **29**, 320–329.
- OGAWA, M., SCHUBERT, G. & ZEBIB, A. 1991 Numerical simulations of three-dimensional thermal convection in a fluid with strongly temperature-dependent viscosity. *J. Fluid Mech.* **233**, 299–328.
- OLIVER, D. S. & BOOKER, J. R. 1983 Planform of convection with strongly temperature dependent viscosity. *Geophys. Astrophys. Fluid Dyn.* **27**, 73–85.
- RICHTER, F. M., NATAF, H.-C. & DALY, S. F. 1983 Heat transfer and horizontally-averaged temperature of convection with large viscosity variations. *J. Fluid Mech.* **129**, 173–192.
- SCHUBERT, G., TURCOTTE, D. L. & OXBURGH, E. R. 1969 Stability of planetary interiors. *Geophys. J. R. Astron. Soc.* **18**, 441–460.
- SMITH, M. K. 1988 Thermal convection during the directional solidification of a pure liquid with variable viscosity. *J. Fluid Mech.* **188**, 547–570.
- SPARROW, E. M., HUSAR, R. B. & GOLDSTEIN, R. J. 1970 Observations and other characteristics of thermals. *J. Fluid Mech.* **41**, 793–800.
- STENGEL, K. C., OLIVER, D. S. & BOOKER, J. R. 1982 Onset of convection in a variable viscosity fluid. *J. Fluid Mech.* **120**, 411–431.
- THOMAS, D. B. & TOWNSEND, A. A. 1957 Turbulent thermal convection over a heated horizontal surface. *J. Fluid Mech.* **2**, 473–485.
- TOWNSEND, A. A. 1959 Temperature fluctuations over a heated horizontal surface. *J. Fluid Mech.* **5**, 209–241.
- TOWNSEND, A. A. 1964 Natural convection in water over an ice surface. *Q. J. R. Met. Soc.* **90**, 248–259.
- WHITE, D. B. 1988 The planforms and onset of convection with a temperature dependent viscosity fluid. *J. Fluid Mech.* **191**, 247–286.
- WRAY, F. 1978 Some convective flows of geophysical interest. PhD thesis, University of Cambridge.